Nanomedicine: Nanotechnology, Biology, and Medicine
14 (2018) 1315–1324

nanomedicine
Nanotechnology, Biology, and Medicine

nanomedjournal.com

Intratumoral evaluation of 3D microvasculature and nanoparticle distribution using a gadolinium-dendron modified nano-liposomal contrast agent with magnetic resonance micro-imaging

Nobuhiro Nitta, MEng[a,b,c], Yoichi Takakusagi, PhD[a,b], Daisuke Kokuryo, PhD[d], Sayaka Shibata, PhD[a,b], Akihiro Tomita, MD, PhD[e], Tatsuya Higashi, MD, PhD[a], Ichio Aoki, PhD[a,b,*], Masafumi Harada, MD, PhD[c]

[a]*National Institute of Radiological Sciences (NIRS), National Institutes for Quantum and Radiological Science and Technology (QST), Chiba, Japan*
[b]*Group of Quantum-state Controlled MRI, QST, Chiba, Japan*
[c]*Graduate School of Medicine, Tokushima University, Tokushima, Japan*
[d]*Graduate School of System Informatics, Kobe University, Kobe, Hyogo, Japan*
[e]*Department of Hematology, Fujita Health University School of Medicine, Toyoake, Aichi, Japan*

Received 3 December 2017; accepted 25 March 2018

Abstract

The enhanced permeability and retention (EPR) effect is variable depending on nanoparticle properties and tumor/vessel conditions. Thus, intratumoral evaluations of the vasculature and nanoparticle distribution are important for predicting the therapeutic efficacy and the intractability of tumors. We aimed to develop a tumor vasculature evaluation method and high-resolution nanoparticle delivery imaging using magnetic resonance (MR) micro-imaging technology with a gadolinium (Gd)-dendron assembled liposomal contrast agent. Using the Gd-liposome and a cryogenic receiving coil, we achieved 50-μm isotropic MR angiography with clear visualization of tumor micro-vessel structure. The Gd-liposome-enhanced MR micro-imaging revealed differences in the vascular structures between Colon26- and SU-DHL6-grafted mice models. The vessel volumes and diameters measured for both tumors were significantly correlated with histological observations. The MR micro-imaging methods facilitate the evaluation of intratumoral vascularization patterns, the quantitative assessment of vascular-properties that alter tumor malignancy, particle retentivity, and the effects of treatment.

Key words: Liposomal contrast agent; Tumor heterogeneity; Angiography; MRI; EPR

Abbreviations: ANOVA, analysis of variance; DAB, diaminobenzidine; DDS, drug delivery system; EPR, enhanced permeability and retention; FOV, field of view; Gd, gadolinium; MIP, maximum intensity projection; MRA, magnetic resonance angiography; MRI, magnetic resonance imaging; MRmA, magnetic resonance micro-angiography; MSME, multi-slice multi-echo; NEX, number of excitations; RARE, rapid acquisition with relaxation enhancement; RF, radiofrequency; ROI, region of interest; RTK, receptor tyrosine kinase; SE, standard error; SD, standard deviation; SNR, signal-to-noise ratio; TE, echo time; TR, repetition time; USPIO, ultra-small superparamagnetic iron oxide nanoparticles.

Conflicts of Interest: The authors declare no potential conflicts of interest.

Research Grant: This research was supported by the Center of Innovation Stream grant and a P-CREATE grant from the Japan Agency for Medical Research and Development. This research was partly supported by Kakenhi grant (#17H00860) awarded by Ministry of Education, Culture, Sports, Science and Technology, Japan.

Acknowledgements: The authors thank the late Dr. Kenji Kono for the development of the Gd-liposome contrast agent. The authors would also like to thank Dr. Jeff Kershaw for English language revision and Ms. Sayaka Hayashi for the cell culture and for animal care.

*Corresponding author at: National Institute of Radiological Science (NIRS), National Institutes for Quantum and Radiological Science and Technology (QST), Chiba, 263-8555, Japan.

E-mail addresses: aoki.ichio@qst.go.jp, iaoki.jp@gmail.com. (I. Aoki).

https://doi.org/10.1016/j.nano.2018.03.006

Tumorigenesis is characterized by abnormal rapid cell proliferation and subsequent microvessel formation from the surrounding host vasculature, which delivers the nutrients and oxygen required for rapid growth. Tumor microvessels often exhibit an architecturally and functionally abnormal structure, which results in a poor supply of oxygen to the cells distant from the vasculature, and induces areas of low oxygen concentration, a state known as hypoxia.[1,2] These heterogeneous tumor micro-environments with insufficient blood flow lead to poor nanoparticles delivery, and hypoxia of cancer cells can reportedly confer anti-tumor drug resistance.[2,3] Nano-platforms have been developed to improve drug delivery specificity in tumor to maximize the chemotherapeutic effect and minimize the side-effect. There were many trials and debates for the enhanced permeability and retention (EPR) effect in tumors[4,5] and it has been clear that the EPR effect is variable depending on multiple factors of the nanoparticle properties and tumor/vessel conditions, such as aberrant vascular architecture, basement membrane disruption, and distribution of stroma cells or fibrosis.[6–8] In addition, cytotoxicity and resistant to radiotherapy also depends on the tumor vasculature, especially presence of oxygen.[1,9] Therefore, research aimed at achieving a better characterization of tumor micro-environments, including associated heterogeneity, is important with regard to identifying and characterizing tumors. Moreover, the assessment of tumor micro-environments *in vivo* is necessary in order to optimize nano-drug selection for treatment and to avoid delivery deficiency to the tumor due to the existence of interstitial cells[8] or vessel impermeability.[10]

Magnetic resonance imaging (MRI) can provide non-invasive and high spatial resolution *in vivo* 3D anatomical information, and magnetic resonance angiography (MRA) using the time-of-flight technique can be used to visualize some broad arteries in humans and animals.[11–14] Higher magnetic field and low-noise radiofrequency (RF) coil technologies enhance the signal-to-noise ratio (SNR) and facilitate increased spatial resolution. There are many *ex vivo* magnetic resonance (MR) micro-imaging techniques that yield spatial resolution of approximately 20–60 μm in animal tissue.[15] However, *in vivo* visualization of intratumoral vessel structure remains a challenge because the resolution of conventional 3D MRA is insufficient for the visualization of intratumoral vessel structure in detail. In addition, it is difficult to ascertain 3D vascularization patterns correctly via tumor tissue sections using optical microscope, because sequential thin sectioning without distortion is technically limited. If *in vivo* MRA with higher resolution is achieved, 3D information derived from the entire tumor without distortion could be obtained and used to evaluate tumor malignancy longitudinally, as well as the therapeutic efficacy of treatment.

The utilization of a drug delivery system (DDS) for cancer diagnostic agents is one of the approaches used to visualize tumor micro-environments.[3] Many types of nanoparticles have reportedly been used for cancer diagnosis.[8,12,13,16] We developed a highly sensitive liposomal contrast agent, PEGylated gadolinium (Gd)-DOTA-dendron-liposome[17] (Gd-liposome), and the agent is provided for research use (Cat # KH16000590, DS pharma biomedical, Osaka, Japan). The Gd-liposome has many Gd-DOTA molecules on its surface, in a dendritic branch configuration.[17] One dendron lipid can have five to eight Gd-DOTA moieties, and the relaxivity is 2.5 times higher than that of the conventional Gd-DOTA.[17] The Gd-liposome (110 nm, averaged diameter) also incorporates PEG, which increases its blood half-life. Due to these characteristics, the Gd-liposome can be expected to accumulate in some types of tumors due to the EPR effect, facilitating their visualization and the determination of their distribution. In addition, the longer half-life in the blood stream can allow for a longer MRI scanning time to obtain a better SNR and spatial resolution.

The aims of this study were to develop a 3D tumor vasculature evaluation method and a high-resolution nanoparticle delivery imaging using MR micro-imaging technology with a Gd-dendron assembled liposomal nanoparticle contrast agent. The PEGylated Gd-liposome was administered intravenously to colon cancer and lymphoma-cells grafted models and differences were analyzed in tumor vessel structures using MR micro-angiography (MRmA). The tumor vasculature information acquired via MRmA was compared to histological sections acquired via vascular endothelial cell-stained microscopic data. The Gd-liposome-enhanced MR micro-imaging methods were then applied to monitor the particle retentivity in tumors and the therapeutic efficacy of an anti-angiogenic agent.

Methods

Ethics statement

Mice were maintained in accordance with the guidelines of the National Institute of Radiological Sciences (NIRS), and all experiments were reviewed and approved by the NIRS committee for the care and use of laboratory animals.

Animal and cell line preparation and tumor treatment

Male BALB/c nude mice (n = 18, 6–10 weeks old, Japan SLC Inc., Shizuoka, Japan) and male NOG© mice (n = 15, 6–10 weeks old, Central Institute for Experimental Animals, Kanagawa, Japan) were prepared. Colon26 tumor cells (murine rectal cancer, 1.0×10^6 cells/50 μL) were subcutaneously transplanted to the gluteal region of BALB/c nude mice (n = 18). As a malignant lymphoma model, SU-DHL6 cells (CD20-positive human origin malignant lymphocytes, 3.0×10^6 cells/50 μL) were transplanted to the gluteal region of NOG© mice (n = 15).[18–20] The two types of mice were randomly divided into three groups, MRI observation with Gd-liposome using cryogenic coil (n = 5), sunitinib treatment (n = 5), and vehicle control (n = 5). In addition, as conventional methods, MRI with Gd-DOTA (gadoterate meglumine, 50 mM, 200 μL/25 g, Terumo, Japan) using a cryogenic coil (n = 1), MRI with Gd-DOTA using the single-loop surface coil (n = 1), and MRI with Gd-liposome using the single-loop surface coil (n = 1) were acquired. The tumors were left to grow to a volume of approximately 150 mm^3 (*i.e.*, 7–8 days after tumor inoculation in Colon26 and 21–25 days in SU-DHL6) for the MRI measurement and 100 mm^3 (*i.e.*, 6–7 days after tumor inoculation in Colon26 and 17–20 days in SU-DHL6) for the therapeutic experiments, respectively.

To evaluate the therapeutic effect and MRmA detection, the anti-angiogenic agent sunitinib and vehicle control solution were prepared. The sunitinib solution was formulated sunitinib (Selleck Pharmaceuticals, Houston, TX, USA) with 0.5% methylcellulose (Nacalai Tesque, Kyoto, Japan) and 0.5% Tween-80 (Nacalai tesque) in attenuated distilled water. The vehicle control solution was prepared using the same solvent without sunitinib. The sunitinib (50 mg/kg) or vehicle control solution was administrated perorally to Colon26-grafted BALB/c nude mice (n = 5 for sunitinib, n = 5 for vehicle control) for 11 days or SU-DHL6-grafted NOG© mice (n = 5 for sunitinib, n = 5 for vehicle control) for 20 days every day. The endpoint of the study was set to 800 mm^3 of tumor volume and the mice that reached the endpoint were euthanized (n = 2 at the vehicle control). The tumor size was calculated with the following formula;

$$\text{Tumor volume} = a \times b \times c \times \pi/6$$

where a and b are the horizontal diameters and c is the depth of the grafted tumor. For tumor volume comparison, the "treated tumor volume ratio" during sunitinib treatment was calculated by: [mean tumor volume of the sunitinib treatment group] / [mean tumor volume of the vehicle control group].

In addition, the tumor doubling time was calculated using the following equation;

$$t_d = \ln 2/\mathrm{SGR}$$
$$\mathrm{SGR} = \ln(V_2/V_1)/(t_2-t_1)$$

where t_d is the tumor doubling time, SGR is the specific tumor growth rate, V is tumor volume, and t is time. The SGR was calculated as the slope value of logarithm regression of the longitudinal tumor volume alteration.

One of the Colon26-grafted BALB/c nude mice was used for longitudinal MRmA observation of the therapeutic effect with an anti-angiogenic agent. The longitudinal MRmA acquisition during treatment was conducted on the day of the initiation of treatment and 7 and 10 days after the initiation of treatment.[21]

MRI measurements and Gd-liposome administration

MR experiments were performed using a preclinical 7 Tesla 20-cm bore MRI system (BioSpec, Avance-III system, Bruker Biospin, Ettlingen, Germany) with a highly sensitive cryogenic RF coil (Cryoprobe©, Bruker Biospin).[22] The coil element and preamplifier in the cryogenic RF coil were cooled by helium gas to suppress thermal noise, so that the SNR using the coil would be approximately 2.5 times higher than that achieved via a conventional RF coil.[22] A single-loop conventional surface coil (20-mm diameter for reception, Rapid Biomedical, Germany) was partly used as a conventional method for SNR comparison. During the *in vivo* MRI experiments, mice (MRI observation group, Colon26-grafted BALB/c nude mice (n = 5) and SU-DHL6-grafted NOG© mice (n = 5)) were anesthetized with 2.0% isoflurane gas (Escain, Mylan, PA, USA) and a 1:5 = O_2: room-air mixture. Rectal temperature was measured via an optical fiber thermometer (FOT-L, FISO Technology, Quebec City, QC, Canada) inserted into the rectum, and maintained at 36.5 ± 0.5 °C via a warm water pad and warm air heating system. Body temperature and breathing were monitored via a Biopac system (BIOPAC Systems, Goleta, CA, USA).

Three types of MR images were acquired. MRmA for visualizing vascular structures in the tumors was acquired using a "fast low angle shot (FLASH)" sequence with the following imaging parameters: repetition time (TR)/echo time (TE) = 15/2.5 ms, field of view (FOV) = 12.8 mm^3, matrix size = 256 × 256 × 256, flip angle = 20°, number of excitations (NEX) = 3, and scan time = 36 min 51 sec. The voxel size was 50 μm^3 isotropic. MRmA images were acquired before and after intravenous (*i.v.*) Gd-liposome administration via the tail vein.[12,23] Gd-liposome (106.3 ± 11.0 nm, averaged diameter measured using dynamic light scattering, ZEN3600, Malvern Instruments, Malvern, United Kingdom) was used to visualize vasculatures in the tumors. The Gd-liposome dose was 23 μmol/kg [Gd] in a 100-μL solution.

Multi-slice T1-weighted images (T1W) to check for particle leakage from the vessels were acquired using a multi-slice multi-echo (MSME) sequence. The imaging parameters used were TR/TE = 400/10 ms, FOV = 19.2 × 13.5 mm, matrix = 256 × 192, slice thickness = 0.78 mm without slice gap, NEX = 4, and scan time = 5 min 7 sec. Multi-slice T2-weighted images (T2W) to investigate tumor anatomy were acquired using a rapid acquisition with relaxation enhancement (RARE) sequence. The imaging parameters used were TR/TE = 3500/40 ms, RARE factor = 8, FOV = 19.2 × 13.5 mm, matrix = 256 × 256, acquisition matrix size = 256 × 192 (Zero-Fill Acceleration = 1.34), slice thickness = 0.75 mm without slice gap, NEX = 2, and scan time = 2 min 48 sec. In all images, a fat-saturated pulse was used to exclude chemical-shift artifacts.

Image analysis and statistical analysis

All MR images were analyzed using MRVision (Version 1.6.8, MRVision, Winchester, MA) and Osirix (Apple Inc. Cupertino, CA, USA)[24] image analysis software. The mean intratumoral vascular diameters for each tumor type were calculated via MRA images. MRA images were binarized using a 50% intensity threshold,[25] the total area of the white regions of the binary map was measured using MRVision, and vasculature diameters were measured using Osirix software. To calculate vascular density, the tumor "periphery" area was defined as the ring-shaped area from the tumor boundary to 3 mm into the coronal slices of the T2W MR images. The tumor "core" was defined as the inner area of the tumor that did not include the periphery.

The statistical analyses of MRA and histological staining were performed using Student's unpaired *t*-test for two-group comparisons (Excel, Microsoft, WA, USA). One-way analysis of variance (ANOVA) with Tukey's correction (GraphPad Prism, Ver. 5, GraphPad Software, Inc., CA, USA) was used for comparisons of vascular properties and two-way ANOVA with Tukey's correction (GraphPad Prism) was used for evaluation of the therapeutic effect for sunitinib. A significance level of $p < 0.05$ was used.

Histological analysis

Immediately after MRI scanning, the mice in the MRI observation group were euthanized and their tumors were excised. The tumors were then embedded in paraffin and sliced

in an axial direction (5 μm in thickness). After deparaffinization for diaminobenzidine (DAB) staining, sections were treated with 10 mM citrate buffer (pH 6.0) and autoclaved at 121 °C for 10 min. After treatment with 3% H_2O_2-methanol for 30 min to remove intrinsic peroxidase and blocking of nonspecific binding sites with 3% bovine serum albumin, in phosphate-buffered saline for 30 min, the slides were probed with antibodies specific for CD31 (rabbit polyclonal, Abcam plc., Cambridge, UK), a blood endothelial cell marker, for 60 min at room temperature.[26] The sections were then incubated with HRP Labelled Polymer Anti-Rabbit (EnVision+© System, Dako Corp. (Agilent), CA, USA) for 30 min at room temperature, and colored with DAB.[27] To evaluate the area of vascular endothelial cells for histological staining, five slices in CD31-stained images were randomly selected. CD31-positive areas were binarized using the Macscope© software (Mitani Corp., Tokyo, Japan), and the proportion of the positive-stained area in the tumor was calculated.

Results

Visualization of murine tumor vasculature in vivo

Figure 1, *A* and *B* shows the representative maximum intensity projection (MIP) images of the Colon26 and SU-DHL6 tumors when tumors grew to approximately 150 mm^3 (7.5 ± 1.3 days on Colon26, 21.2 ± 3.3 days on SU-DHL6, respectively) (Figure 1, *C*). Blood vessels with diameters of approximately 50 μm and above could be visualized clearly in both types of xenografts, using MRmA with Gd-liposome. The vascular structures in the two tumor models differed considerably. In Colon26 tumors, the thin blood vessels were predominantly located in the peripheral part and were relatively sparse in the core (Figure 1, *A*, Supplementary Video 1). Conversely, the cores of the SU-DHL6 malignant lymphomas contained numerous large vessels with many thin branches (Figure 1, *B*, Supplementary Video 1). Figure 1, *D* shows intratumoral vessel volumes calculated via the MIP images. The mean vessel volumes were 2.45 ± 0.42 mm^3 for Colon26 tumors and 3.78 ± 0.89 mm^3 for SU-DHL6 tumors, indicating that SU-DHL6 tumors had a larger volume of blood vessels than Colon26 tumors. MRAs using conventional methods at the same 7 T-MRI scanner were also obtained as follows; MRmA acquired with a cryogenic RF coil after Gd-DOTA *i.v.* injection (Figure 1, *E*), MRmA acquired with the single-loop surface coil (20-mm diameter) after Gd-DOTA *i.v.* injection (Figure 1, *F*), and MRmA acquired with the single-loop surface coil after Gd-liposome *i.v.* injection (Figure 1, *G*). The MRA images acquired with Gd-DOTA were blurry and tumor vessel structure was ambiguous (Figure 1, *E* and *F*). Although the Gd-liposome specifically enhanced vessel structure, the conventional single-loop surface coil lacked in SNR for thin vessels (Figure 1, *G*).

Quantitative analysis of tumors vascularization patterns via MRmA images

To better understand the differences in vascular properties between the two tumor types, their vascularization patterns were quantitatively analyzed. Figure 2 shows typical 3D MRmA MIP and binarized images on the coronal plane (red). As shown in Figure 2, *A*, blood vessels were mainly located on the surface of Colon26 tumors, while density was low in the core part. In contrast, blood vessels were widely observed throughout the SU-DHL6 tumors (Figure 2, *B*). The vascular areas in the core and peripheral parts of tumors were quantified via coronal sections of each MRmA image, and the results are shown in Figure 2, *C*. In Colon26 tumors, the mean vascular area in the core part was 0.55 ± 0.35 μm^2, while in the peripheral part it was 4.54 ± 1.23 μm^2, suggesting that Colon26 preferentially forms tumor vasculature in the peripheral part. In contrast, in SU-DHL6 tumors the mean vascular areas were 4.03 ± 0.58 μm^2 in the core part and 5.36 ± 4.73 μm^2 in the peripheral part, suggesting that tumor vessels grow uniformly throughout SU-DHL6 tumor tissues.

Evaluation of vascular diameter via MRmA images

The MRmA images were further used to evaluate the differences in vascular diameters. Figure 3, *A* shows typical whole 2D images (upper), and a "zoomed in" image of vessel signal and region of interest (ROI) line for the measurement of vessel diameters (bottom). Figure 3, *B* shows vessel diameter values of Colon26 and SU-DHL6 tumors derived from 3D MRmA images. The mean vessel diameters were 97.0 ± 8.2 μm for Colon26 tumors and 145.0 ± 10.5 μm for SU-DHL6 tumors, and this difference was statistically significant ($n = 5$, $p < 0.05$).

The vessel diameter was also measured from CD31 immunohistological images and compared between both tumors. As shown in Figure 3, *C*, the CD31-positive zone in the peripheral area (the white square in the MRmA image) was detected (bottom). The diameter of the intravascular space in SU-DHL6 was 1.5 ± 0.1 fold larger than that of colon26 (Figure 3, *D*), indicating a significant difference between Colon26 and SU-DHL6 tumors, as is the case with the MRmA results shown in Figure 3, *B*. Figure 3, *E* shows the CD31-positive area measured using an optical microscope. The mean CD31-positive areas were 0.33 ± 0.13% in Colon26 tumors and 0.75 ± 0.16% in SU-DHL6 tumors, and this difference was statistically significant. This result was concordant with the difference in vascular density that was noninvasively assessed via MRmA (Figure 1, *D*).

Evaluation of therapeutic effect of an anti-angiogenic agent via MRmA images

Figure 4, *A* and *B* shows the growth kinetics of Colon26 (A) and SU-DHL6 (B) xenografts during the treatment. The treatment with sunitinib (50 mg/kg/day) suppressed the growth significantly both in Colon26 (11 days after beginning of treatment, $p < 0.05$) and SU-DHL6 tumors (9–21 days after beginning of treatment, $p < 0.05$, 0.01, or 0.001). At day 10, the treated tumor volume ratio to the control of SU-DHL6 (0.44, Figure 4, *B*, solid square) was smaller than that of Colon26 (0.69, Figure 4, *A*, solid square), suggesting that SU-DHL6 is more sensitive to anti-angiogenic therapy compared to colon26. Figure 4, *C* and *D* shows the logarithmic regression to calculate tumor doubling time of Colon26 (C) and SU-DHL6 (D) xenografts with or without the treatment. The tumor doubling time in Colon26 was 3.27 days ($R^2 = 0.98$) in the control group and 4.25 days ($R^2 = 0.93$) in the treatment group. On the other hand, the doubling time in SU-DHL6 was 7.26 days ($R^2 = 0.98$) in the control group and 9.63 days ($R^2 = 0.97$) in the treatment group.

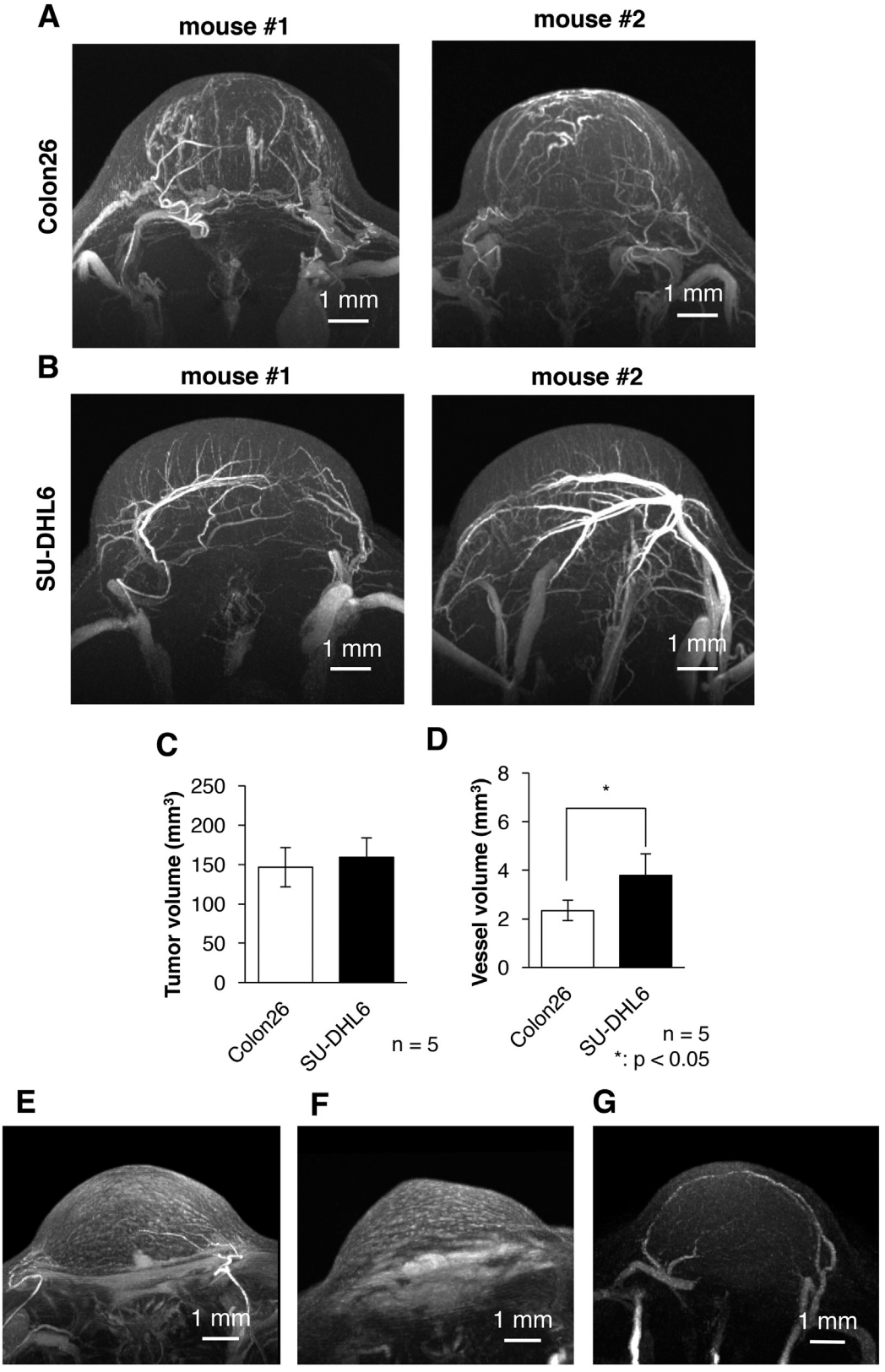

Figure 1. Representative MIP images of murine tumor xenografts constructed MRmA. **(A)** MIP image of MRmA in two different Colon26 transplant model mice. **(B)** MIP image of MRmA in two different SU-DHL6 transplant model mice. **(C)** Tumor volume calculated via the anatomical image on MRmA. The data shown are means ± SD (n = 5). **(D)** Intratumor vessel volumes calculated via MRmA images. The data shown are means ± SD (n = 5). **(E)** MRmA acquired with a cryogenic RF coil after Gd-DOTA *i.v.* injection, **(F)** MRmA acquired with the single-loop surface coil (20-mm diameter) after Gd-DOTA *i.v.* injection, **(G)** MRmA acquired with the single-loop surface coil after Gd-liposome *i.v.* injection. *$p < 0.05$.

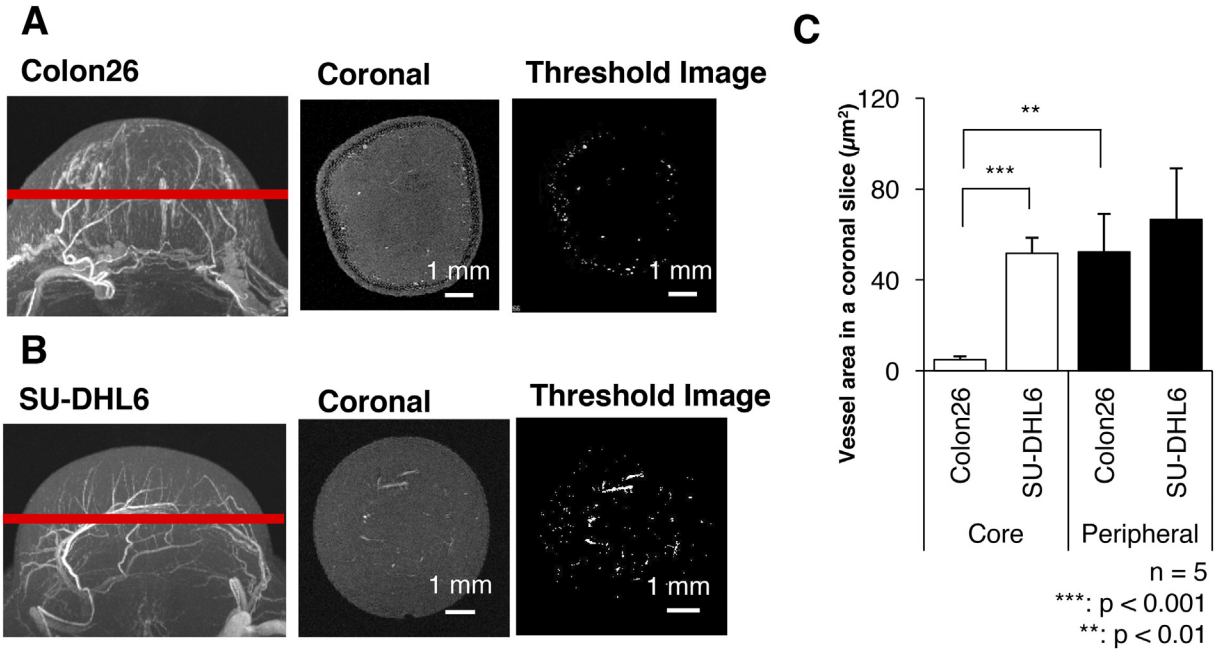

Figure 2. Vessel distribution analysis in the core and peripheral parts in coronal slices of each tumor type. **(A)** Colon26. **(B)** SU-DHL6. 3D MIP (left), 2D magnitude (middle), and threshold (right) images are shown. The red bar on the 3D MIP image represents the position of the coronal slice. **(C)** Vessel areas in the core and peripheral parts calculated via coronal sections. The data shown are means ± SD (n = 5), and one-way ANOVA was used to conduct statistical comparisons. $^{**}p < 0.01$, $^{***}p < 0.001$.

Longitudinal imaging assessment of treatment response to an anti-angiogenic agent

Figure 5 shows MRmA MIP and T1W images acquired in conjunction with the administration of the Gd-liposome contrast agent over a time-course of sunitinib treatment. As indicated within the white circles (Figure 5, MRmA, Supplementary Video 2), diminished and vague vessel contrast were observed on days 7 and 10 compared with pre-treatment. Furthermore, partial signal enhancement at the treated tumors both in the T1W images and MRmA was observed, indicating leakage of the nanoparticles contrast agent from vessels and accumulation into tumor tissues immediately after the administration. Collectively, these results suggest that anti-angiogenic effects and nanoparticles distribution on murine tumor xenografts can be noninvasively monitored via MRmA.

Discussion

Clear visualization of intratumoral vasculature using the Gd-liposome-enhanced MRmA

MRA is highly beneficial with regard to obtaining anatomical large vessel information.[11,12,28–31] However, the quantitative evaluation of intratumoral vascular properties is difficult due to limited resolution. The present study using Gd-liposome with MR micro-imaging technology achieved 50 μm isotropic resolution MRmA, which enabled the quantitative assessment of tumor vasculature volume and diameter. The particle size of Gd-liposome is approximately 110 nm, and is less leaky than the intact vasculature, and the PEGs on the surface extend its blood half-life by 4–8 hours. These characteristics facilitate retention of the Gd-liposome in blood pools during MRmA scanning, which was clearly visible in tumor vasculature on the MR images. On the other hand, smaller molecular weight contrast agents, which are used clinically, often leak from both normal and abnormal capillaries into tissues, resulting in the generation of low contrast images (Figure 1, *E*).

In addition, the Gd-liposome provided high contrast because the surface of the Gd-liposome has high dense Gd-DOTA conjugation, due to the many dendritic branches, and could achieve high relaxivity (2.5 times of Gd-DOTA). Furthermore, the combined use of a highly sensitive cryogenic radiofrequency coil (SNR per 1 mm^3: 34,110 at copper sulfate phantom, Bruker Biospin) on 7 T MRI further assisted the increase in the resolution of MR images compared to the use of a single loop surface coil (SNR per 1 mm^3: 9056). The use of suitable combinational micro-imaging technologies using blood-pool nanoparticles with high density and relaxivity capabilities and high SNR coils acted synergistically to increase resolution and the SNR of MR imaging.

Note that the Gd-liposome-enhanced MRmA and MIP visualization could detect the arterioles and venules (100–200 μm in diameter) but could not detect the capillaries and very small vessels (under 50 μm). For evaluation of the capillaries, perfusion MRI methods, such as arterial spin labeling or the dynamic contrast-enhanced method, will be useful, although it is impossible to visualize single capillaries.

Significance in noninvasive evaluation of intratumoral vascular architecture

Vascularization patterns and vascular diameters differ in each tumor type. Contrary to normal vessels, the tumor vasculature

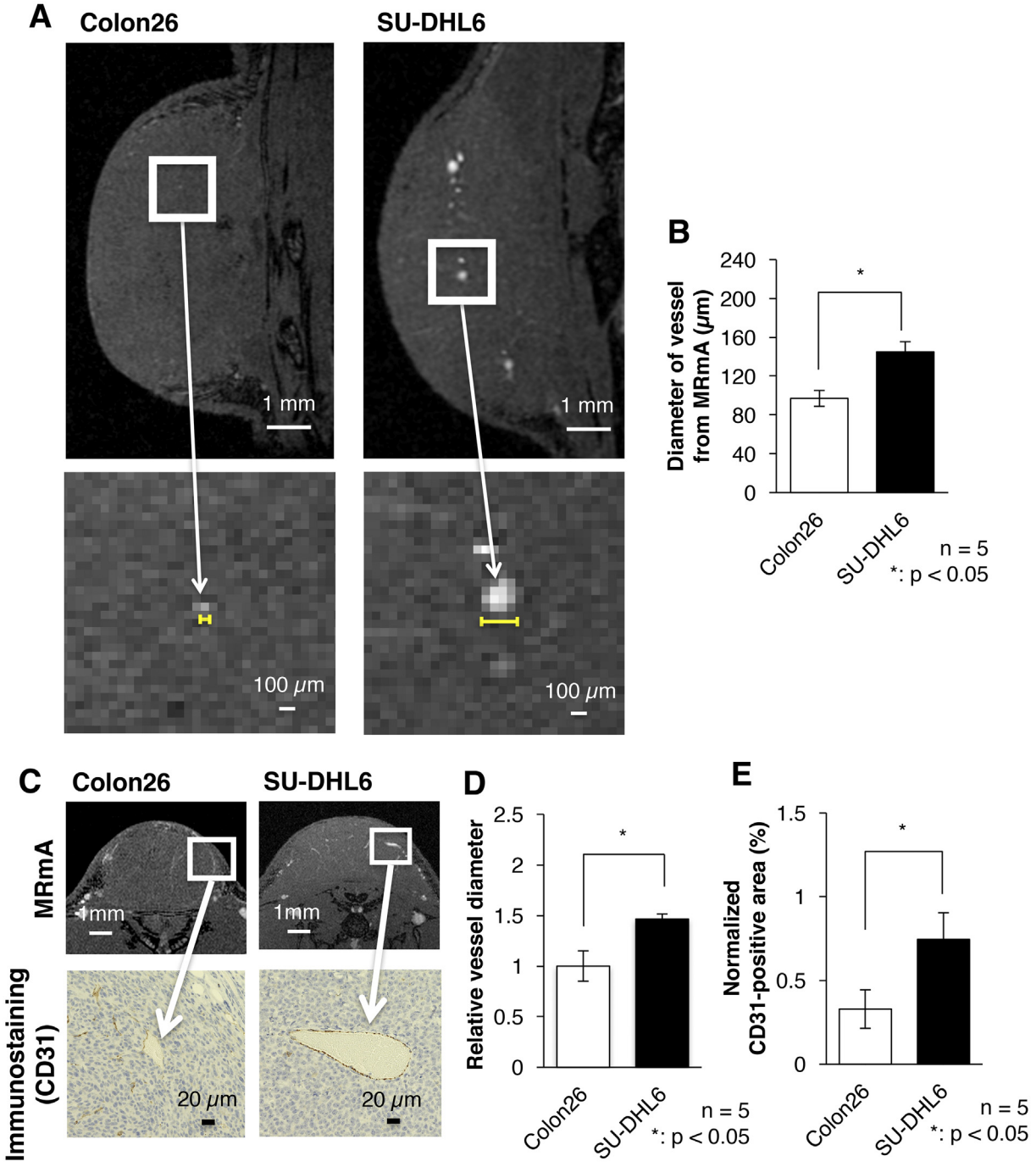

Figure 3. Comparison of vascular properties of Colon26 and SU-DHL6 tumors *in vivo* as determined via magnetic resonance imaging and histological staining. **(A)** 2D sagittal slices (upper) and enlarged maps (white squares in the sagittal images) of Colon26 and SU-DHL6 tumors. **(B)** Diameter of blood vessels measured via magnetic resonance micro-angiography. The data shown are means ± SD (n = 5). **(C)** Representative MRmA images of each tumor type (upper) and histological staining of tumor sections. The images correspond to the white square in each corresponding MRmA image. The blood endothelial cell marker CD31 was stained with diaminobenzidine. **(D)** Relative diameter of blood vessels measured from CD31 histological staining (n = 5). *$p < 0.05$. **(E)** Quantification of CD31-positive areas as determined via histological images (n = 5). *$p < 0.05$.

pattern is extremely disorganized and anarchic and presents morphological and structural differences, *i.e.*, weak association between endothelial cells, abnormal shapes of pericytes, lack of smooth muscles, as well as basal membrane modification.[10,16] Ryschich *et al.* reported that malignant tumors have thick blood vessels correlated with malignancy for supply to tumor tissue.[32] Thus, the noninvasive assessment of vascular properties is useful for the diagnosis of tumorigenesis or its malignant transformation.

In addition to the vascular architecture, whether the EPR effect occurs in the tumor has a great influence on the strategy of nanomedicine. Indeed, we have previously reported that PEGylated liposome (approximately 110 nm) can gradually accumulate in tumors

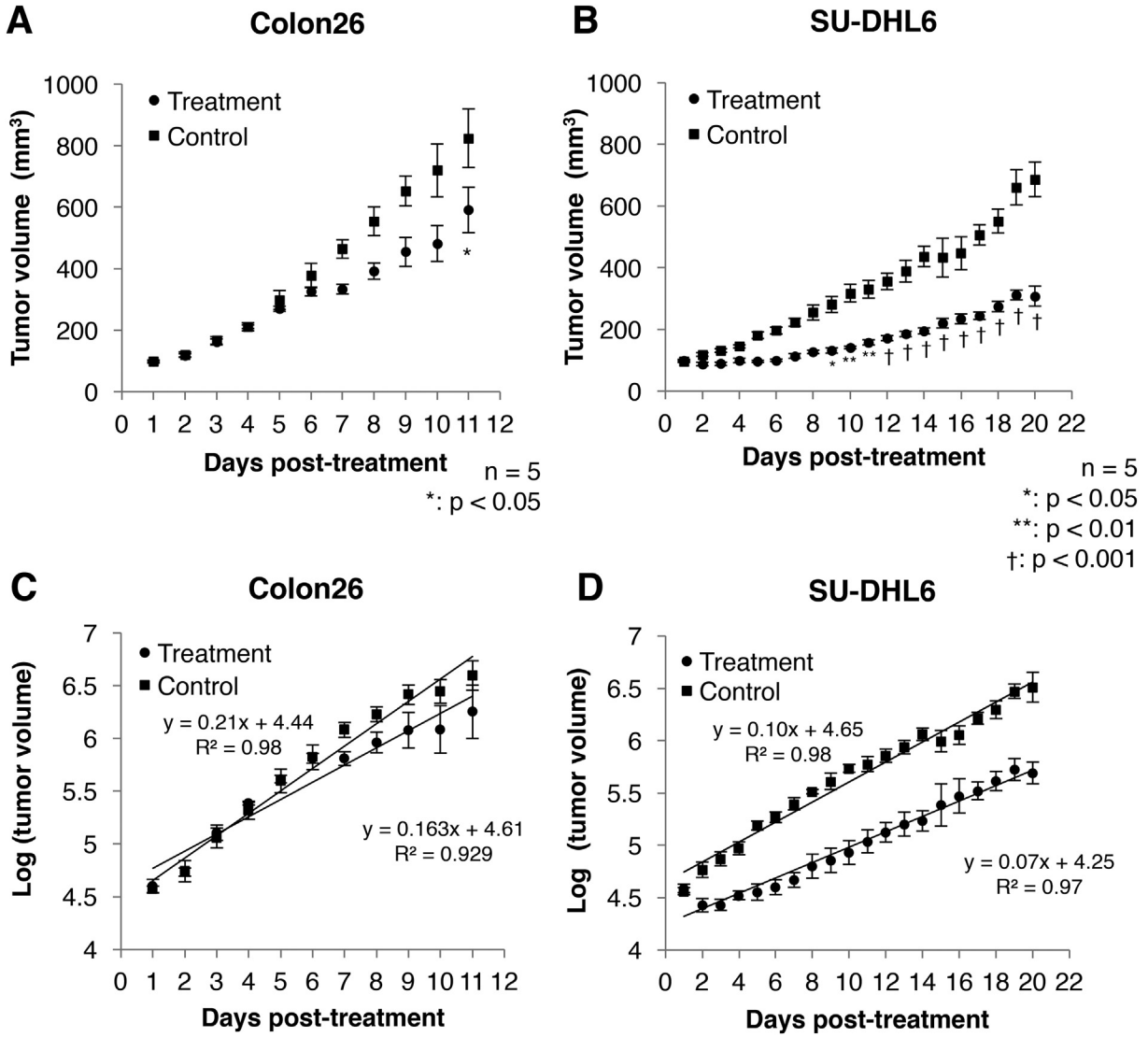

Figure 4. Longitudinal tumor volume alteration during sunitinib treatment. Colon26 and **(B)** SU-DHL6 were presented. To calculate the tumor doubling time, the natural logarithmic scale and the regressions for **(C)** Colon26 and **(D)** SU-DHL6 are also presented. Solid circles indicate sunitinib treatment group, and solid squares mean vehicle only control group, respectively. The data shown means ± SE (n = 5). *$p < 0.05$, **$p < 0.01$, †$p < 0.001$.

due to the EPR effect for 4–8 hours.[17,33,34] In addition to the late phase EPR effect, MRmA and T1W MR micro-images, after the anti-angiogenic therapy, could detect leakage of the Gd-liposomal nanoparticles from vessels and accumulation into tumor tissues immediately after the administration (Figure 5). It should be noted that evaluation of tumor vasculature (volume, density, patterning, and diameter) and accumulation of nanoparticles on MRI allows assessment of the tumoral microenvironment and its heterogeneity when it is combined with other functional MR measurements, such as T1W image (Figure 5), diffusion (Supplementary Figure 1), perfusion, blood oxygenation level dependent, and other nanoparticles-enhanced MR images.

Noninvasive evaluation of anti-angiogenic chemotherapy on the high resolution MRmA

Folkman *et al.* first proposed the essential role of angiogenesis in tumor growth in 1971.[35,36] He studied the process by which a tumor attracts blood vessels to nourish itself and sustain its existence on tumor angiogenesis.[37] Starting from those achievements, many effective drugs have been developed, such as molecular target therapy.[27,38–40] Among them, sunitinib was developed as an anti-angiogenic agent, which inhibits multiple receptor tyrosine kinase (RTK).[41] Krishna *et al.* evaluated the time course changes of relative tumor vessel volume with MRI in combination use with ultra-small superparamagnetic iron oxide nanoparticles (USPIO), a negative contrast agent, upon sunitinib treatment.[38] In this study, Gd-liposome-enhanced 3D MRmA clearly distinguished the differences in vascular properties between colon26 and SU-DHL6. This positively enhanced contrast of blood vessels allowed measurement of the absolute tumor vessel volume (mm^3) (Figure 1, *D*) and provided evidence that sunitinib is more effective for SU-DHL6 than for colon26. Indeed, sunitinib administration was predominantly beneficial for the treatment of SU-DHL6 tumors (Figure 4) in which vessel

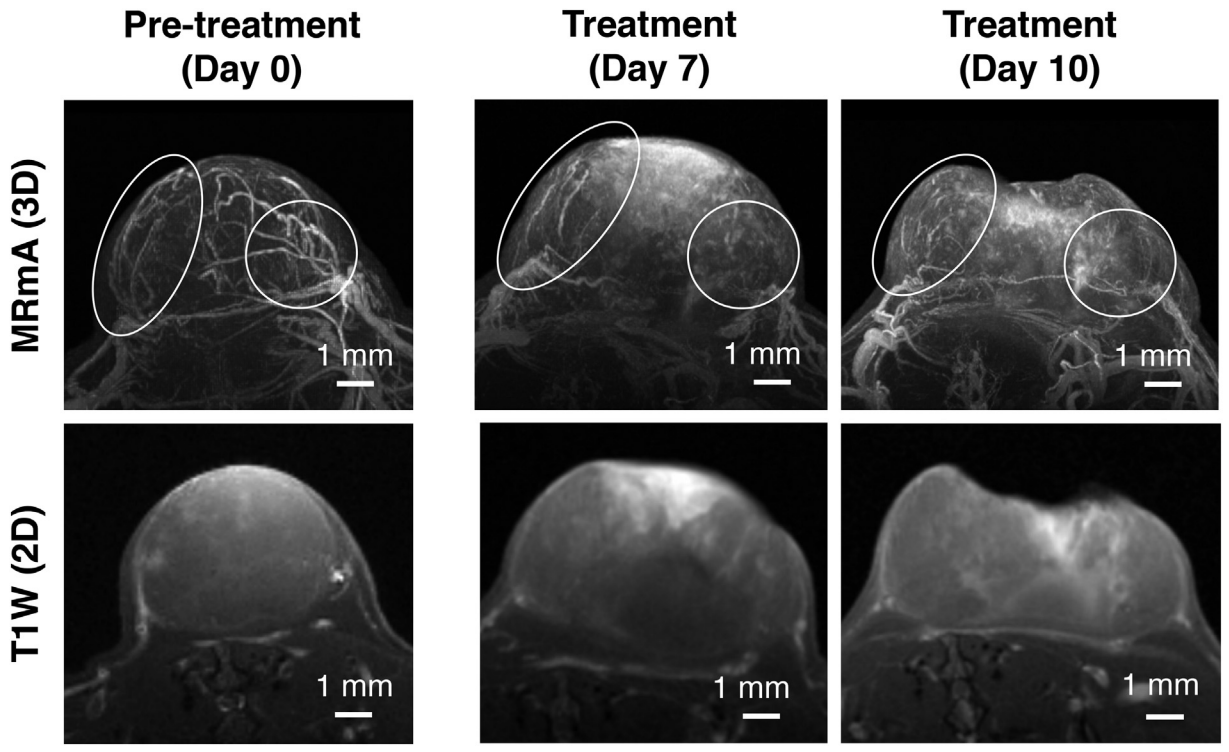

Figure 5. Profiling of Colon26 tumor vascular alterations via MRmA after anti-angiogenic therapy. MIP images derived via MRmA (upper) and T1W images (lower) before treatment and 7 and 10 days after daily treatment with sunitinib are shown.

density and diameter were greater than in colon26 (Figure 1, *D*). In addition, our method also allowed monitoring of the spatial and temporal alterations of tumor vasculature upon sunitinib treatment (Figure 5, Supplementary Video 2). Thus, more precise evaluation of intratumoral vasculature is possible using our 3D MRmA, which enables the decision of the appropriate treatment method and on follow-up whether the anti-angiogenic therapy is effective and should be continued.

In conclusion, we developed a 3D tumor vasculature evaluation method and a high-resolution nanoparticle delivery imaging using MR micro-imaging technology with a Gd-dendron assembled liposomal nanoparticle contrast agent. The Gd-liposome-enhanced 3D MRmA technology revealed differences in the vascular structures between Colon26 and SU-DHL6 (malignant lymphoma) grafted models and facilitated the longitudinal observation of therapeutic alterations. The MR micro-imaging methods facilitate the evaluation of intratumoral vascularization patterns, the quantitative assessment of vascular properties that alter tumor malignancy, particle retentivity in tumors, and the effects of treatment. We expect that the 3D MR micro-imaging methods described herein will prove widely applicable for the *in vivo* evaluation of tumor heterogeneity and the fine prediction for nanomedicine following additional development of therapeutic nanoparticles and theranostic agents in the future.

Appendix A. Supplementary data

Supplementary data to this article can be found online at https://doi.org/10.1016/j.nano.2018.03.006.

References

1. Thomlinson RH, Gray LH. The histological structure of some human lung cancers and the possible implications for radiotherapy. *Br J Cancer* 1955;**9**(4):539-49.
2. Barker HE, Paget JT, Khan AA, Harrington KJ. The tumour microenvironment after radiotherapy: mechanisms of resistance and recurrence. *Nat Rev Cancer* 2015;**15**(7):409-25.
3. Bennett KM, Jo J, Cabral H, Bakalova R, Aoki I. MR imaging techniques for nano-pathophysiology and theranostics. *Adv Drug Deliv Rev* 2014;**74**:75-94.
4. Matsumura Y, Maeda H. A new concept for macromolecular therapeutics in cancer chemotherapy: mechanism of tumoritropic accumulation of proteins and the antitumor agent smancs. *Cancer Res* 1986;**46**(12):6387-92.
5. Maeda H, Nakamura H, Fang J. The EPR effect for macromolecular drug delivery to solid tumors: Improvement of tumor uptake, lowering of systemic toxicity, and distinct tumor imaging in vivo. *Adv Drug Deliv Rev* 2013;**65**(1):71-9.
6. Bertrand N, Wu J, Xu X, Kamaly N, Farokhzad OC. Cancer nanotechnology: the impact of passive and active targeting in the era of modern cancer biology. *Adv Drug Deliv Rev* 2014;**66**:2-25.
7. Cabral H, Matsumoto Y, Mizuno K, Chen Q, Murakami M, Kimura M, et al. Accumulation of sub-100 nm polymeric micelles in poorly permeable tumours depends on size. *Nat Nanotechnol* 2011;**6**(12):815-23.
8. Kano MR, Bae Y, Iwata C, Morishita Y, Yashiro M, Oka M, et al. Improvement of cancer-targeting therapy, using nanocarriers for intractable solid tumors by inhibition of TGF-beta signaling. *Proc Natl Acad Sci U S A* 2007;**104**(9):3460-5.
9. Camphausen K, Moses MA, Beecken WD, Khan MK, Folkman J, O'Reilly MS. Radiation therapy to a primary tumor accelerates metastatic growth in mice. *Cancer Res* 2001;**61**(5):2207-11.

10. Azzi S, Hebda JK, Gavard J. Vascular permeability and drug delivery in cancers. *Front Oncol* 2013;**3**(211):1-14.
11. Kobayashi H, Sato N, Kawamoto S, Saga T, Hiraga A, Ishimori T, et al. 3D MR angiography of intratumoral vasculature using a novel macromolecular MR contrast agent. *Magn Reson Med* 2001;**46**(3):579-85.
12. Radbruch A, Eidel O, Wiestler B, Paech D, Burth S, Kickingereder P, et al. Quantification of tumor vessels in glioblastoma patients using time-of-flight angiography at 7 Tesla: a feasibility study. *PLoS One* 2014;**9**(11)e110727.
13. Yang CT, Chandrasekharan P, He T, Poh Z, Raju A, Chuang KH, et al. An intravascular MRI contrast agent based on Gd(DO3A-Lys) for tumor angiography. *Biomaterials* 2014;**35**(1):327-36.
14. Brubaker LM, Bullitt E, Yin C, Van Dyke T, Lin W. Magnetic resonance angiography visualization of abnormal tumor vasculature in genetically engineered mice. *Cancer Res* 2005;**65**(18):8218-23.
15. Norris FC, Siow BM, Cleary JO, Wells JA, De Castro SC, Ordidge RJ, et al. Diffusion microscopic MRI of the mouse embryo: Protocol and practical implementation in the splotch mouse model. *Magn Reson Med* 2015;**73**(2):731-9.
16. Kobayashi H, Watanabe R, Choyke PL. Improving conventional enhanced permeability and retention (EPR) effects; what is the appropriate target? *Theranostics* 2013;**4**(1):81-9.
17. Kono K, Nakashima S, Kokuryo D, Aoki I, Shimomoto H, Aoshima S, et al. Multi-functional liposomes having temperature-triggered release and magnetic resonance imaging for tumor-specific chemotherapy. *Biomaterials* 2011;**32**(5):1387-95.
18. Tokunaga T, Tomita A, Sugimoto K, Shimada K, Iriyama C, Hirose T, et al. De novo diffuse large B-cell lymphoma with a CD20 immunohistochemistry-positive and flow cytometry-negative phenotype: molecular mechanisms and correlation with rituximab sensitivity. *Cancer Sci* 2014;**105**(1):35-43.
19. Miyoshi H, Arakawa F, Sato K, Kimura Y, Kiyasu J, Takeuchi M, et al. Comparison of CD20 expression in B-cell lymphoma between newly diagnosed, untreated cases and those after rituximab treatment. *Cancer Sci* 2012;**103**(8):1567-73.
20. Wada N, Aozasa K. Loss of CD20 expression after rituximab therapy for b-cell lymphomas: a review of the literature. *Cancer Clin Oncol* 2012;**1**(2):1-9.
21. Ma X, Wang L, Li H, Zhang Y, Gao Y, Guo G, et al. Predictive immunohistochemical markers related to drug selection for patients treated with sunitinib or sorafenib for metastatic renal cell cancer. *Sci Rep* 2016;**6**:1-11.
22. Niendorf T, Pohlmann A, Reimann HM, Waiczies H, Peper E, Huelnhagen T, et al. Advancing cardiovascular, neurovascular, and renal magnetic resonance imaging in small rodents using cryogenic radiofrequency coil technology. *Front Pharmacol* 2015;**6**(255):1-21.
23. Saito S, Aoki I, Sawada K, Sun XZ, Chuang KH, Kershaw J, et al. Quantitative and noninvasive assessment of prenatal X-ray-induced CNS abnormalities using magnetic resonance imaging. *Radiat Res* 2011;**175**(1):1-9.
24. Rosset A, Spadola L, Ratib O. OsiriX: an open-source software for navigating in multidimensional DICOM images. *J Digit Imaging* 2004;**17**(3):205-16.
25. Otake M. Review: Radiation-related brain damage and growth retardation among the prenatally exposed atomic bomb survivors. *Int J Radiat Biol* 2009;**74**(2):159-71.
26. Newman JM, Dora KA, Rattigan S, Edwards SJ, Colquhoun EQ, Clark MG. Norepinephrine and serotonin vasoconstriction in rat hindlimb control different vascular flow routes. *Am J Physiol* 1996;**270**(4):E689-99.
27. Takakusagi Y, Matsumoto S, Saito K, Matsuo M, Kishimoto S, Wojtkowiak JW, et al. Pyruvate induces transient tumor hypoxia by enhancing mitochondrial oxygen consumption and potentiates the anti-tumor effect of a hypoxia-activated prodrug TH-302. *PLoS One* 2014;**9**(9)e107995.
28. Johst S, Orzada S, Fischer A, Schafer LC, Nassenstein K, Umutlu L, et al. Sequence comparison for non-enhanced MRA of the lower extremity arteries at 7 Tesla. *PLoS One* 2014;**9**(1)e86274.
29. Lee YB, Kang CK, Kim KT, Park CA, Kim YB, Cho ZH. A non-invasive technique for visualization of microvessels in asymptomatic patients with middle cerebral artery steno-occlusion. *Vasc Med* 2013;**18**(5):314-7.
30. Zhang H, Maki JH, Prince MR. 3D contrast-enhanced MR angiography. *J Magn Reson Imaging* 2007;**25**:13-25.
31. Runge VM, Kirsch JE, Lee C. Contrast-enhanced MR angiography. *JMRI* 1993;**3**(1):233-9.
32. Ryschich E, Schmidt E, Maksan S-M, Klar E, Schmidt J. Expansion of endothelial surface by an increase of vessel diameter during tumor angiogenesis in experimental hepatocellular and pancreatic cancer. *World J Gastroenterol* 2004;**10**(21):3171-4.
33. Gabizon A, Papahadjopoulos D. Liposome formulations with prolonged circulation time in blood and enhanced uptake by tumors. *Med Sci* 1988;**85**(18):6949-53.
34. Woodle MC, Lasic DD. Sterically stabilized liposomes. *Biochim Biophys Acta* 1992;**1113**(2):171-99.
35. Folkman J, Merler E, Abernathy C, Williams A. Isolation of a tumor factor responsible for angiogenesis. *J Exp Med* 1971;**133**(2):275-88.
36. Ausprunk DH, Knighton DR, Folkman J. Vascularization of normal and neoplastic tissues grafted to the chick chorioallantois. *Am J Pathol* 1975;**79**(3):597-617.
37. Cao Y, Langer R. A review of Judah Folkman's remarkable achievements in biomedicine. *Proc Natl Acad Sci USA* 2008;**105**(36):13203-5.
38. Matsumoto S, Saito K, Takakusagi Y, Matsuo M, Munasinghe JP, Morris HD, et al. In vivo imaging of tumor physiological, metabolic, and redox changes in response to the anti-angiogenic agent sunitinib: longitudinal assessment to identify transient vascular renormalization. *Antioxid Redox Signal* 2014;**21**(8):1145-55.
39. Kyutoku M, Nakagami H, Koriyama H, Tomioka H, Nakagami F, Shimamura M, et al. Development of novel DNA vaccine for VEGF in murine cancer model. *Sci Rep* 2013;**3**:1-7.
40. Osawa T, Tsuchida R, Muramatsu M, Shimamura T, Wang F, Suehiro J, et al. Inhibition of histone demethylase JMJD1A improves anti-angiogenic therapy and reduces tumor-associated macrophages. *Cancer Res* 2013;**73**(10):3019-28.
41. Chow LQ, Eckhardt SG. Sunitinib: from rational design to clinical efficacy. *J Clin Oncol* 2007;**25**(7):884-96.